eprints@whiterose.ac.uk
https://eprints.whiterose.ac.uk/

1st Virtual European Conference on Fracture

Single cylinder subjected to vortex-induced vibrations: estimating cyclic stresses for fatigue assessment

Daniel Mella[a,*], Wernher Brevis[b], Luca Susmel[a]

[a]*Department of Civil and Structural Engineering, The University of Sheffield, Sheffield S102TG, UK*
[b]*Department of Hydraulics and Environmental Engineering and Department of Mining Engineering, Pontifical Catholic University of Chile, Santiago 3580000, Chile*

Abstract

This study estimates the cyclic (i.e. fatigue) stresses on a pivoted cylinder subjected to a range of fully developed turbulent flows. The tested cylinder configuration allowed to transfer the complex fluid-structure interaction forces to a bottom-fixed stainless steel rod through a rigid connection. Thus, a direct relationship between the cylinder motion and the maximum stresses on the rod was established. The cylinder motion was recorded using a high-speed camera and its temporal position determined by means of the Digital Image Correlation technique. The results showed a dominant crossflow response with an oscillation frequency equal to half the oscillation frequency in the streamwise direction. Nevertheless, the total streamwise stress was 158 MPa, which was on average 11% lower compared to the total crossflow stress. Despite having dominant crossflow response, the higher oscillation frequency and comparable maximum stress in the streamwise direction showed that both directions should be considered for fatigue damage assessment.

Keywords: Vortex-induced vibrations; Fatigue; Digital image correlation; Cyclic stress

1. Introduction

Vortex-induced vibrations (VIV) is a nonlinear, self-governed, multi-degree-of-freedom (DOF) phenomenon (Sarpkaya (2004)) that occurs due to the interaction between the vortex formation behind a body and its structural response. The complex three-dimensional forces exerted by these vortices can potentially induce body motions which, in turn, modifies the vortex shedding process itself. This constant feedback can be an important contributor to fatigue damage and structural instability in numerous engineering problems,

* Corresponding author. Daniel Mella. Department of Civil and Structural Engineering, The University of Sheffield, Mappin Street, S1 3JD, Sheffield, UK. Telephone: 0114 222 2000.
   E-mail address: mvamellavivanco1@sheffield.ac.uk

such as marine risers, bridges, towers, masts, heat exchanger tubes, submerged floating tunnels, to name a few. The responses and oscillation frequencies of a cylinder subjected to VIV have received considerable attention in the past few decades. The mass ratio (m^*), defined as the structural mass divided by the displaced fluid mass, has an impact on the range of flow velocities in which the cylinder exhibits significant body motions (Khalak and Williamson (1997)). Likewise, The product between m^* and the structural damping ratio (ζ), called mass-damping ratio, controls the maximum cylinder displacement (Khalak and Williamson (1997)). The range of significant body motions is called synchronisation range and is characterised by a vortex shedding frequency equal to the cylinder oscillation frequency (Williamson and Govardhan (2004)). These results were obtained for cylinders restricted to move perpendicular to the flow direction. However, higher displacements and new vortex patterns were observed when the cylinder was free to vibrate along (streamwise) and perpendicular (crossflow) to the flow direction. The crossflow motion only is referred to as one degree-of-freedom, while the streamwise and crossflow response is called two degrees-of-freedom. Jauvtis and Williamson (2004) compared the vortex shedding and structural response between a one degree-of-freedom and a two degree-of-freedom cylinder. When $m^* > 6$, the additional degree-of-freedom had a small impact in the maximum displacement and vortex patterns. However, at lower m^*, maximum amplitudes of $1.5D$ in the crossflow direction and maximum oscillations of $0.3D$ in the streamwise direction were observed. Here, D is the cylinder diameter. Previous studies showed an interdependence between the streamwise and crossflow responses (Vandiver and Jong (1987)). Flemming and Williamson (2005) studied the response of a two degrees-of-freedom cylinder and found that high oscillations on the streamwise direction enhance the maximum crossflow amplitudes.

Fatigue analysis on structures subjected to VIV is usually conducted using in-field or large scale laboratory tests. Measurement techniques, such as accelerometers, pressure sensors, and strain gauges, are commonly used to characterise the structural response (see, for example, Trim et al. (2005); Wang et al. (2015)). When the experimental set-up requires small scale models, one effective method to induce significant responses is by testing light-weight cylinders. Sensor placement on these structures could change its dynamic properties and, thus, its fluid-structure interaction. Moreover, multiple sensors are required to characterise the complex VIV forces in order to estimate the total stresses on a structure. This work employed a non-contact measurement system to determine the cyclic (i.e. fatigue) stresses on a pivoted cylinder subjected to VIV. The pivoted cylinder was composed by a clear cast acrylic tube, a 316l stainless steel rod placed inside the acrylic tube, and a rigid connection that ensured a monolithic behaviour between the acrylic tube and the rod. Thus, a direct relationship between the cylinder response and the stresses on the rod was established. The pivoted cylinder was subjected to a range of flow velocities from 0.11 to 0.29 m/s. A high-speed camera was mounted on top of the acrylic tube and recorded its response at 70 Hz for 90 seconds. The cylinder position was estimated using the Digital Image Correlation technique. The cylinder response was characterised in terms of maximum amplitudes, their associated stresses, and main oscillation frequencies.

2. Experimental setup

The experiments were performed at the Civil and Structural Engineering water laboratory, University of Sheffield, United Kingdom. The flume was covered with clear cast acrylic sheets leaving a squared cross-sectional area of 255 mm width and a longitudinal fixed slope of 0.001 m/m. A water depth of $H_{\mathrm{w}} = 240$ mm was fixed using a computer-controlled system. The mean incoming flow velocities U_{in} ranged from 0.11 to 0.29 m/s (maximum flow rate of the facility), corresponding to a reduced flow velocity U_{r} between 2.26 to 5.87. Here, $U_{\mathrm{r}} = U_{\mathrm{in}}/(f_{\mathrm{nw}}D)$, where f_{nw} is the natural frequency of the structure measured in still water, and D is the diameter of the cylinder. The incoming turbulent intensity was measured at 5% for all tested flow velocities. A pivoted cylinder was fixed at 10.5 m downstream the entrance of the flume. The structure was composed of a clear cast acrylic tube, a 316l stainless steel solder rod, and a rigid plug that ensured a monolithic behaviour between the rod and acrylic tube. Figure 1 shows a sketch of the pivoted cylinder with its dimensions. The acrylic tube of 1.19 g/cm^3 had an outer diameter of $D = 20$ mm, 4 mm thickness, and 300 mm length. The stainless steel rod had a diameter $D_{\mathrm{p}} = 1.5$ mm and length $L_{\mathrm{p}} = 150$ mm. The material of the rod had an ultimate tensile and yield stress of $\sigma_{\mathrm{UTS}} = 544$ Mpa and $\sigma_{\mathrm{Yield}} = 245$ Mpa,
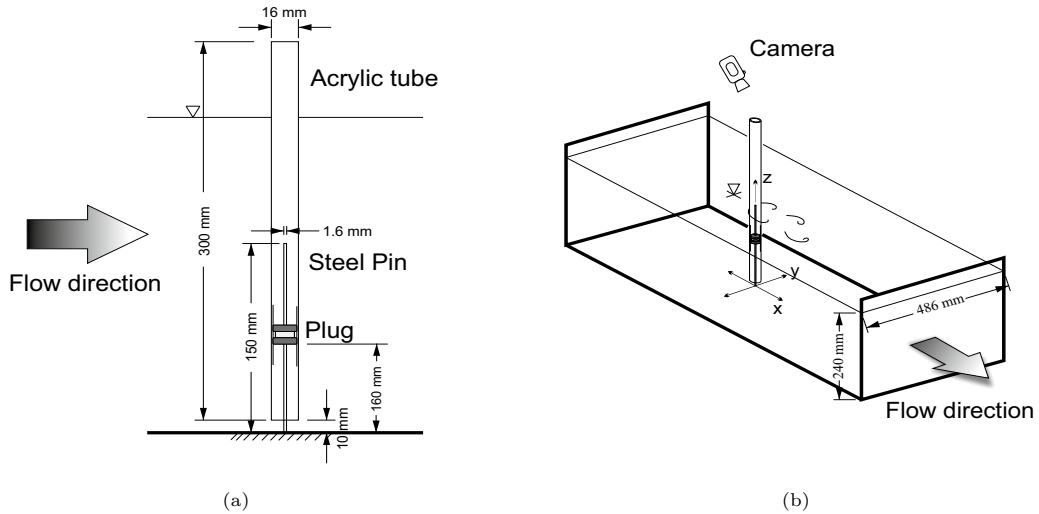
Fig. 1: Experimental setup of a pivoted cylinder subjected to a range of turbulent flows. Cylinder oscillations in crossflow (y-axis) and streamwise (x-axis) directions. The z-axis lies along the span of the cylinder. a) Side view. b) three-dimensional view.

respectively (Huang et al. (2006)). The rigid plug weighted 5 g with a 15 mm height. The distance between the acrylic tube and the bottom of the flume was 10 mm. Likewise, the distance between the plug and the bottom of the flume was 70 mm. The pivoted cylinder was chemically fixed to an acrylic sheet of 10 mm thickness. This configuration allowed the structure to freely oscillate in the streamwise (x-axis) and crossflow (y-axis) direction. The total oscillating structure had $m^* = 1.48$. A 4M MX camera of 2048x2048 pixel resolution was located above the cylinder focusing on its free end. Recordings of its temporal position were taken at 70 Hz for 90 seconds. The measurements started at $U_r = 2.26$ and was gradually increased after each recording until $U_r = 5.87$. A calibration plate LaVision model 058-5 was used to determine the pixel to real-world transformation and to correct a small inclination angle between the camera and the cylinder free end. Details of the calibration process can be found in Brevis and García-Villalba (2011) and Mella et al. (2019). The cylinder position in each recording was determined using the Digital Image Correlation technique. This image-based tracking technique was implemented using the open-source library OpenPIV (Taylor et al. (2010)).

The structural damping ratio ξ, and the natural frequency measured in air f_{na} and still water f_{nw} were calculated using a free-decay test. The cylinder was subjected to a unidimensional displacement parallel and perpendicular to the flow direction. A camera of eight MegaPixel resolution and 30 Hz acquisition frequency was placed on top of the cylinder recording its motion. A frequency analysis showed that $f_{na} = 2.84$ and $f_{nw} = 2.61$ Hz. A decaying exponential curve fit on the cylinder response estimated ξ at 0.39%. These dynamic parameters were not affected by the direction of the unidimensional displacement. The free decay test was repeated after all the experiments were completed with no degradation of the dynamic properties of the vibrating structure.

3. Cylinder motion to maximum stresses

The pivoted cylinder shown in Figure 1a allowed to transfer the complex fluid-structure interaction forces to a stainless steel rod through a single rigid connection. This configuration ensured a monolithic behaviour between the acrylic tube and the rod. Thus, if the cylinder free end position is given by $\boldsymbol{x}_c = [x(t), y(t)]$, the rod free end position is equal to $\boldsymbol{x}_p = k[x(t), y(t)]$. The reaction moment on the rod $\boldsymbol{M}_p = [M_x, M_y]$ and its corresponding bending stress $\boldsymbol{\sigma} = [\sigma_x, \sigma_y]$ were calculated assuming a linear-elastic response. A numerical model of the cylinder configuration was developed in Ansys Academic Research Structural, Release 18.1.

Four unidimensional displacements were imposed in the cylinder free end $\boldsymbol{x}_c = ([0.5, 1, 1.5, 2], 0)D$, measuring the reaction moment $\boldsymbol{M}_p$ in the fixed end of the stainless steel rod. The ratio $\boldsymbol{M}_p/\boldsymbol{x}_c$ for all tested $\boldsymbol{x}_c$ was 3.88. Thus, the bending stresses associated to a given displacement $\boldsymbol{x}_c$ was calculated as

$$\boldsymbol{\sigma} = \frac{3.88\boldsymbol{x}_c D}{2I} \tag{1}$$

where $I = \pi D^4/64$ is the moment of inertia.

4. Results

4.1. Cylinder response
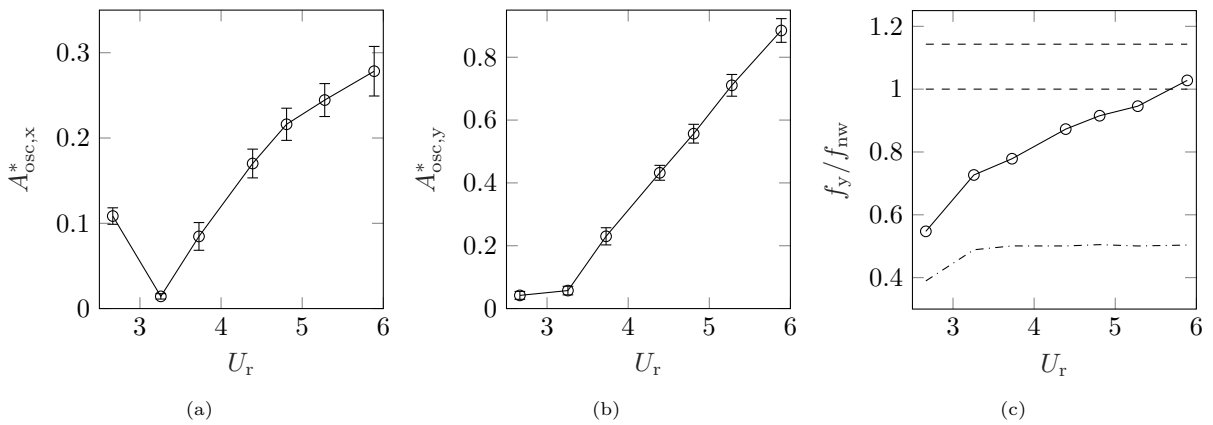
Fig. 2: Maximum response and oscillation frequency of a pivoted cylinder subjected to $2.26 \leq U_r \leq 5.87$. a) Maximum streamwise response, error bars: $A^*_{\text{osc,x}} \pm \text{SD}_x$. b) Maximum crossflow response, error bars: $A^*_{\text{osc,y}} \pm \text{SD}_y$. c) Crossflow oscillation frequency
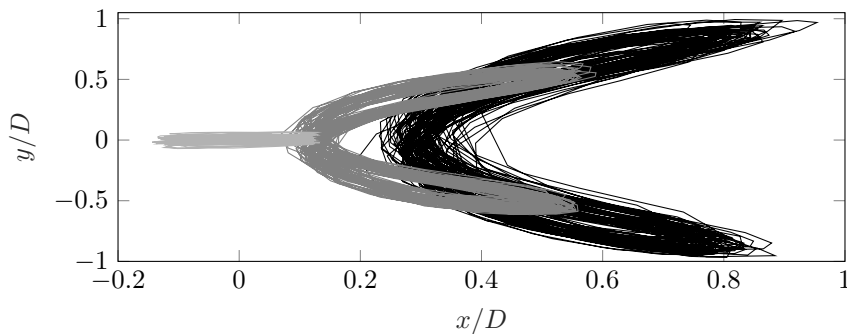
Fig. 3: Cylinder trajectory at different U_r. ▬: $U_r = 2.67$, ▬: $U_r = 4.81$. ▬: $U_r = 5.89$

Figure 3 shows the trajectory traced by the cylinder at different flow velocities. A dominant crescent-type trajectory is observed as U_r increases. The cylinder response in a given direction was decomposed as the sum of an oscillatory $\boldsymbol{A}_{\text{osc}}$ and mean $\overline{\boldsymbol{A}}$ displacement. As shown in Figure 3, $\overline{A}_y \approx 0$, whereas $\overline{A}_x$

increased with U_r. Figure 2a and 2b show the maximum oscillatory response in the streamwise $A^*_{osc,x}$ and crossflow $A^*_{osc,y}$ directions, respectively. The maximum oscillatory response in a given direction was defined as the mean value of the highest 10% of the recorded response, as in Hover et al. (1998). Vertical bars correspond to one standard deviation (SD) around the maximum value. The cylinder response increased with U_r, except for an initial reduction of $A^*_{osc,x}$ at $U_r = 3.24$. The maximum observed responses were $A^*_{osc,x} = 0.28D$ and $A^*_{osc,y} = 0.89D$ at the maximum tested flow velocity. Figure 2c shows the cylinder main oscillation frequency in the crossflow direction f_y. Dashed-dotted lines represent the ratio between the main streamwise and crossflow oscillation frequency, f_y/f_x. Dashed lines enclose f_{nw} and f_{na}. The crossflow oscillation frequency varied between $0.63f_{nw}$ and $1.17f_{nw}$. The ratio f_y/f_x was equal to 0.5 throughout the tested flow velocities, except at the initial $U_r = 2.67$.

4.2. Maximum stresses

(a) ●: Maximum/minimum $\overline{\sigma}_x \pm \sigma^*_{osc,x}$. ▲: mean $\overline{\sigma}_x$

(b) ●: Maximum/minimum $\pm\sigma^*_{osc,y}$.

(c) ▲: $\overline{\sigma}_x + \sigma^*_{osc,x}$. ▲: $\sigma^*_{osc,x}$. ●: $\sigma^*_{osc,y}$
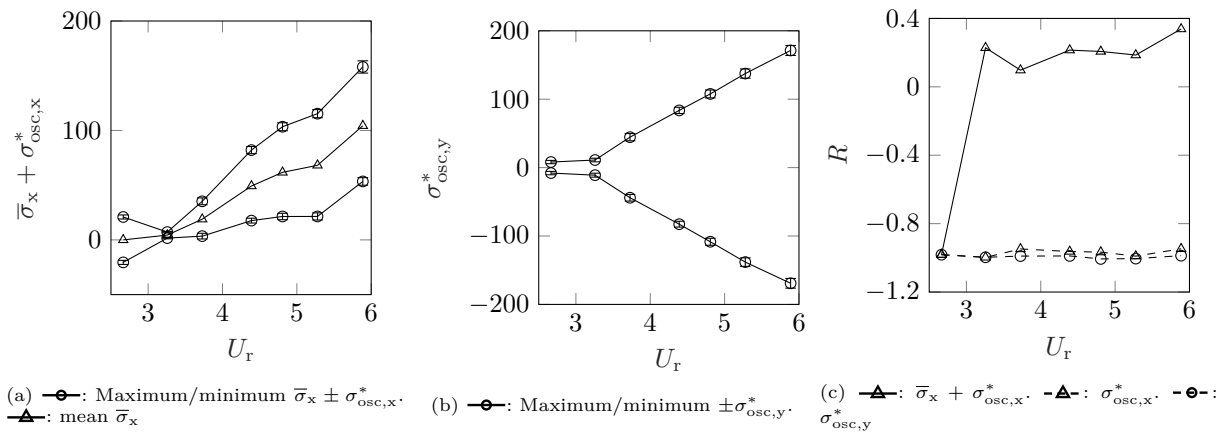
Fig. 4: Bending stresses associated to the maximum responses and stress ratio. a) Streamwise stress, error bars: $\sigma_x \pm SD_x$. b) Crossflow stress, error bars: $\sigma_y \pm SD_y$. c) Stress ratio

Same as in Section 4.1, the stresses in a given direction were decomposed as the sum of a cyclic and mean stresses, $\boldsymbol{\sigma} = \boldsymbol{\sigma}_{osc} + \overline{\boldsymbol{\sigma}}$. $\overline{\sigma}_y \approx 0$, whereas $\overline{\sigma}_x$ increased with U_r. Figure 4a and 4b show the maximum total stresses in the streamwise $(\overline{\sigma}_x + \sigma^*_{osc,x})$ and crossflow $(\sigma^*_{osc,y})$ direction. Here, $\sigma^*_{osc,x}$ and $\sigma^*_{osc,y}$ are the stresses associated with $A^*_{osc,x}$ and $A^*_{osc,y}$, respectively. The maximum $\sigma^*_{osc,x}$ was 52.3 Mpa at the maximum tested U_r. On the other hand, the maximum $\sigma^*_{osc,y}$ was 171 Mpa. Considering the influence of $\overline{\sigma}_x$, the maximum and minimum total stresses in the streamwise direction were 53.4 and 158 Mpa, respectively. These results showed that, despite having a dominant crossflow response $(A^*_{osc,y}/A^*_{osc,x} \approx 3.1)$, the maximum total stress in the streamwise direction was on average only 11% lower than its crossflow counterpart for $U_r \geq 4.39$. The stress ratio, defined as the quotient between the minimum and maximum stress, is shown in Figure 4c. As expected, $R \approx -1$ across U_r for $\sigma^*_{osc,x}$ and $\sigma^*_{osc,y}$. Considering the total streamwise stresses, the stress ratio varied between 0.18 and 0.33 for $U_r \geq 3.28$.

5. Conclusion

This work employed a non-contact measurement system to determine the cyclic (i.e. fatigue) stresses on a pivoted cylinder subjected to VIV. The structural configuration allowed to transfer the complex fluid-structure interaction forces to a bottom-fixed stainless steel rod through a single rigid connection. Thus, a direct relationship between the cylinder motion and the maximum stresses on the rod was established. The results showed a crescent-shape trajectory as the flow velocity increased. The maximum observed responses were 0.28D and 0.89D in the streamwise and crossflow direction, respectively. The main oscillation frequency

in the streamwise direction ranged between $0.63f_{\text{nw}}$ and $1.17f_{\text{nw}}$, which was double the crossflow oscillation frequency. The total stresses on a given direction were decomposed as the sum of a mean and cyclic stresses. The mean streamwise stress increased with the flow velocity, whereas its crossflow counterpart was equal to zero through the tested flow velocities. The total stress in the streamwise was 158 MPa, which was on average 11% lower compared to the total stress in the crossflow direction. The stress ratio of the total streamwise component varied between 0.18 and 0.38. On the other hand, the stress ratio of the cyclic stresses was equal to minus one in both directions. Despite having dominant crossflow response, the higher oscillation frequency and comparable maximum stress in the streamwise direction showed that both directions should be considered for fatigue damage assessment.

Acknowledgements

References

Brevis, W., García-Villalba, M., 2011. Shallow-flow visualization analysis by proper orthogonal decomposition. Journal of Hydraulic Research 49, 586–594. doi:10.1080/00221686.2011.585012.

Flemming, F., Williamson, C.H., 2005. Vortex-induced vibrations of a pivoted cylinder. Journal of Fluid Mechanics 522, 215–252. doi:10.1017/S0022112004001831.

Hover, F.S., Techet, A.H., Triantafyllou, M.S., 1998. Forces on oscillating uniform and tapered cylinders in crossflow. Journal of Fluid Mechanics 363, 97–114. doi:10.1017/S0022112098001074.

Huang, J.Y., Yeh, J.J., Jeng, S.L., Chen, C.Y., Kuo, R.C., 2006. High-Cycle Fatigue Behavior of Type 316L Stainless Steel. Materials Transactions 47, 409–417. doi:10.2320/matertrans.47.409.

Jauvtis, N., Williamson, C.H., 2004. The effect of two degrees of freedom on vortex-induced vibration at low mass and damping. Journal of Fluid Mechanics 509, 23–62. doi:10.1017/S0022112004008778.

Khalak, A., Williamson, C.H., 1997. Investigation of relative effects of mass and damping in vortex-induced vibration of a circular cylinder. Journal of Wind Engineering and Industrial Aerodynamics 37, 341–350. doi:10.1016/S0167-6105(97)00167-0.

Mella, D.A., Brevis, W., Jonathan, H., Racic, V., Susmel, L., 2019. Image-based tracking technique assessment and application to a fluid-structure interaction experiment. Proceedings of the Institution of Mechanical Engineers, Part C: Journal of Mechanical Engineering 233, 5724–5734. doi:10.1177/0954406219853852.

Sarpkaya, T., 2004. A critical review of the intrinsic nature of vortex-induced vibrations. Journal of Fluids and Structures 19, 389–447. doi:10.1016/j.jfluidstructs.2004.02.005.

Taylor, Z.J., Gurka, R., Kopp, G.A., Liberzon, A., 2010. Long-duration time-resolved PIV to study unsteady aerodynamics. IEEE Transactions on Instrumentation and Measurement 59, 3262–3269. doi:10.1109/TIM.2010.2047149.

Trim, A.D., Braaten, H., Lie, H., Tognarelli, M.A., 2005. Experimental investigation of vortex-induced vibration of long marine risers. Journal of Fluids and Structures 21, 335–361. doi:10.1016/j.jfluidstructs.2005.07.014.

Vandiver, J.K., Jong, J.Y., 1987. The relationship between in-line and cross-flow vortex-induced vibration of cylinders. Journal of Fluids and Structures 1, 381–399. doi:10.1016/S0889-9746(87)90279-9.

Wang, J., Fu, S., Baarholm, R., Wu, J., Larsen, C.M., 2015. Fatigue damage induced by vortex-induced vibrations in oscillatory flow. Marine Structures 40, 73–91. doi:10.1016/j.marstruc.2014.10.011.

Williamson, C., Govardhan, R., 2004. Vortex-Induced Vibrations. Annual Review of Fluid Mechanics 36, 413–455. doi:10.1146/annurev.fluid.36.050802.122128.